ADVANCED ENGINEERING MATERIALS
www.aem-journal.com

Plasma-Induced Maskless Formation of Quasi-Periodic Nanoripples on Polymeric Substrates

*Athina S. Kastania, Sotiris Mouchtouris, Eleni Stai, Angelos Zeniou, George Kokkoris, Vassilios Constantoudis, Pavlos Tsavalas, Konstantina Mergia, Evangelos Gogolides, and Angeliki Tserepi**

Quasi-periodic nanostructures on a variety of materials have recently attracted tremendous attention due to their capability to dramatically change the materials' surface performance and enable a variety of applications. In reported studies, materials are nanostructured by "exotic" preparation strategies such as self-assembly, cluster ion beams, and femtosecond lasers, not necessarily providing rapid, large-area, and scalable fabrication based on a widespread technology. Herein, reactive plasma etching is proposed as a conventional technological route for maskless, large-area, and mass production of quasi-periodic nanoripples formed on the bottom, adjacent to the electrode, area of polymeric substrates perpendicularly oriented with respect to the electrode. To provide a justification basis for the proposed strategy, a comprehensive modeling framework is employed for the calculation of particle trajectories, which predict the angular and energy distribution of ions reaching the perpendicular substrate. These distributions show ions impinging on the area adjacent to the electrode with high off-normal angles and high energies, favoring the formation of nanoripples. The density of the formed nanoripples and the degree of their quasi-periodicity are dependent on ion density, processing time, and the polymer material, enabling the control of such plasma-induced periodic surface structures that can be paramount for a wide spectrum of applications.

1. Introduction

Periodic nanostructures on various materials exhibit a wide range of special properties—from optical to electrical—due to their well-defined ordered patterns making them attractive for applications in various fields, such as photonics and optoelectronics,[1] energy conversion and water splitting, photovoltaics and fuel cells,[2] self-cleaning surfaces, and antireflective coatings (windows, paints, etc.).[3] Such periodic nanostructures can be fabricated on a wide range of materials from semi-conductors to metals and polymers with a variety of methods that may not necessarily provide scalability and large-area production. Examples of these methods include short-pulse laser processing, for example, ultraviolet or infrared femtosecond laser irradiation,[4–6] various lithographic techniques, for example, self-assembly of colloidal spheres or multiple-patterning nanosphere lithography,[7,8] growth by oblique angle sputter deposition,[9] roll-to-roll patterning,[10] and plasma etching.[11] The latter method, adapted in the present work, has several advantages over many other methods in terms of combining speed, scaling-up, widespread technology, and maskless fabrication.

More particularly, gaseous plasma treatment, involved in surface engineering of polymeric substrates, combines[12] rapidly and in one-step the ability to control the wetting behavior,[13,14] to tailor optical properties,[15] to enhance the surface area, and to introduce useful chemical functionalities such as carboxyl and carbonyl groups.[16,17] Additionally, plasma

A. S. Kastania, S. Mouchtouris, E. Stai, A. Zeniou, V. Constantoudis, E. Gogolides, A. Tserepi
Institute of Nanoscience and Nanotechnology
NCSR "Demokritos"
153 41 Aghia Paraskevi, Greece
E-mail: a.tserepi@inn.demokritos.gr

The ORCID identification number(s) for the author(s) of this article can be found under https://doi.org/10.1002/adem.202402729.

DOI: 10.1002/adem.202402729

S. Mouchtouris, G. Kokkoris
School of Chemical Engineering
National Technical University of Athens
157 80 Athens, Greece

E. Stai
Department of Physics
National and Kapodistrian University of Athens
15784 Athens, Greece

P. Tsavalas, K. Mergia
Institute of Nuclear & Radiological Sciences and Technology
NCSR "Demokritos"
153 41 Aghia Paraskevi, Greece

treatment enhances the surface biocompatibility, improves the detection sensitivity, and imparts antimicrobial properties to the treated surfaces.[18,19] These modified surfaces have found extensive use as smart and functional substrates, particularly useful when integrated in microfluidic devices.[20,21] The majority of such plasma engineered surfaces contain nanowire-like nanostructures and are processed lying down to the powered electrode, with the ions normally impinging at nearly perpendicular direction on the surface. Nevertheless, rarely in the literature, surfaces are etched with ions impinging at off-normal angles,[22,23] achieved by a modified plasma sheath, and ion beam etching,[24] leading to intriguing geometric features, including wiggling structures and periodic nanoripples.

Herein, the concept of implementing a modified sheath to accelerate ions at high off-normal angles near the bottom edge of a polymeric substrate, by simply placing the substrate in the plasma reactor at right angles with respect to the electrode (**Figure 1**), is proposed and demonstrated. To this end, a modeling framework is employed to predict the formation of anisotropic structures on perpendicularly placed polymeric substrates. The results are also compared to the typical case of polymeric samples horizontally placed on the electrode.

The said framework implements a reactor scale model and a Monte Carlo particle tracing model that calculates the local distributions of the ion incident angles and energies; the latter distributions are found to depend on the distance from the bottom edge of the perpendicularly placed substrate (see Figure 1). Near the bottom edge, the highest impinging ion angles are calculated, indicating that the ions "scratch" the polymeric surface leading to ripple formation, parallel to the ion direction. At increasing distances from the substrate bottom edge, the ion impinging angle decreases, leading to a more isotropic roughened pattern. This interesting phenomenon describing the trend from anisotropic (nanoripples) to isotropic (nanowire-like) roughness pattern is actually confirmed after plasma processing of poly(methyl methacrylate) (PMMA) samples, via scanning electron microscope (SEM) images and their metrological analysis demonstrating the periodicity of the anisotropic pattern. The masklessly formed quasi-periodic nanoripples can actually be exploited in applications from light harvesting by adjusting the optical properties of the materials used[25] to bioanalytical chemistry by controlling the ripple wavelength toward optimization of surface-enhanced raman spectroscopy (SERS) substrates,[26] microfluidics by providing wetting control as well as embedment of SERS surfaces inside the chips[27] and bioengineering. As an example, concerning the latter, surface roughness topographies are shown to influence the differentiation of human mesenchymal stem cells,[28,29] endothelial cells and smooth muscle cells.[30]

2. Results and Discussion

2.1. Computational Analysis and Simulation Explaining the Mechanism of Nanoripple Formation

The aim of the computational analysis is to elucidate whether we can produce anisotropic roughness, that is, ripples, on polymeric substrates by a single plasma etching step, without using a mask or intricate sheath control plates. Based on previous computational[31–35] and experimental[36,37] studies, which show that ripple formation (along the direction of ions) is feasible when ions bombard the surface at angles greater than a critical value, that is, 60° up to 80° depending on the system,[31,33–37] we aimed at finding means to produce ions bombarding the polymeric substrates at such angles, without using intricate sheath control plates. An intuitive choice is to put the substrate perpendicularly on the electrode (see **Figure** 1 and **2**b), thus affecting the sheath developed around the polymeric substrate and consequently the direction of ions. In order to verify that the intuitive choice would be effective, we employ a modeling framework consisting of a reactor scale model[38] and a Monte Carlo particle tracing model,[39] described in the Experimental Section, in order to predict the local ion energy and angular distributions on the polymeric substrate.

The results of the calculations for both a horizontally (Figure 2a,c,e) and a perpendicularly (Figure 2b,d,f) placed substrate (at a radial distance of 80 mm from the reactor center) are portrayed in Figure 2. In Figure 2a,b, the electric potential and the electric field vectors are shown for both cases; these results are derived from the reactor scale model and are used as inputs to the particle tracing model, which calculates the ion trajectories and ultimately the local ion energy distribution

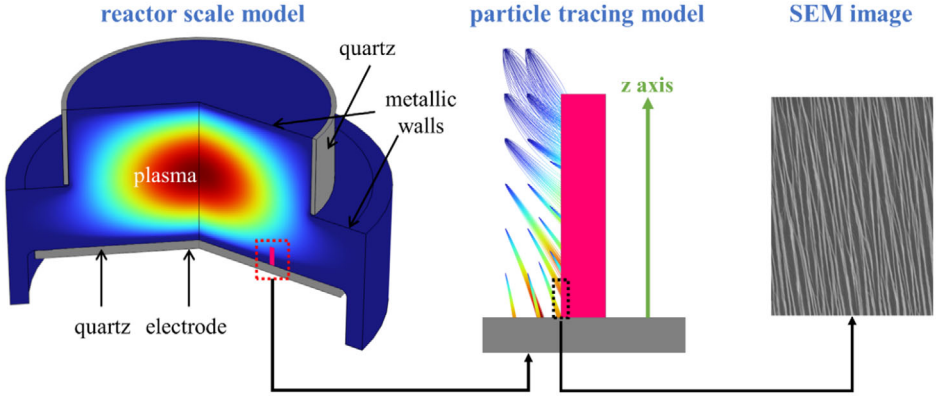

Figure 1. Schematic of the proposed technology and the modeling framework justifying the formation of anisotropic structures (as represented on the SEM image) on polymeric substrates perpendicularly placed on the electrode.

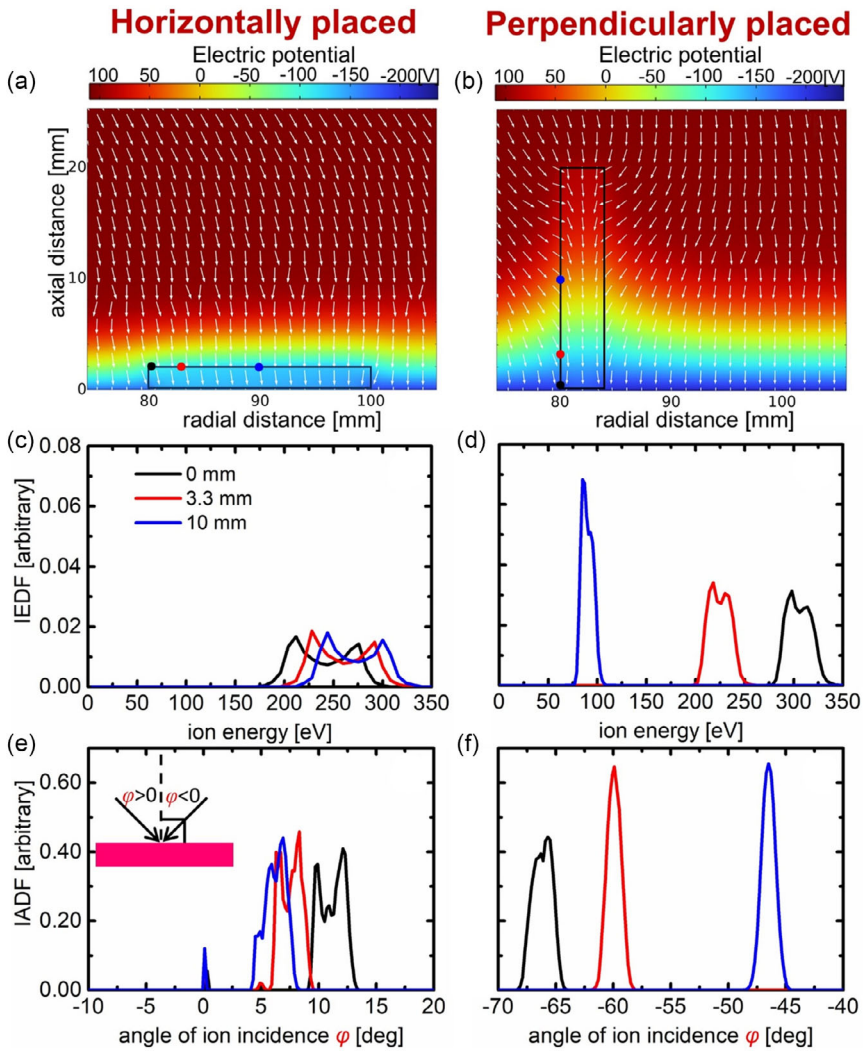

Figure 2. Results of the modeling framework. a,b) The time-averaged electric potential and electric field vector (white arrows) for a polymeric substrate placed horizontally (left column) and perpendicularly (right column) on the electrode. c,d) The IEDFs and e,f) the IADFs at three positions along the polymeric substrate, namely 0, 3.3, and 10 mm away from the bottom edge of the polymeric sample. The operating conditions for the capacitively coupled plasma: 5.2 mTorr, and an applied RF power (at 13.56 MHz) on the electrode achieving a self-bias voltage of −210 V.

functions (IEDFs) and ion angular distribution functions (IADFs). In Figure 2c–f, the local IEDFs and IADFs at distances 0, 3.3, and 10 mm (black, red, and blue points in Figure 2a,b) away from the bottom edge of the polymeric substrate are compared.

In the case of the horizontally placed polymeric sample, the IEDFs at all the positions have almost the same mean energy and shape (Figure 2c). They exhibit the well-known bimodal shape attributed to the relation of the transition time required for ions to cross the plasma sheath in comparison to the electric time period value, that is, very low ratio of transition time to electric field period.[40] The mean energy remains almost the same due to the fact that the electric potential does not change significantly on the surface of the polymeric sample (Figure 2a), that is, the potential difference with the bulk plasma is almost the same at all positions.

In the case of the perpendicularly placed polymeric sample (Figure 2d), a noticeable difference of the IEDFs from the previous case (horizontally placed) is evident. The electric potential increases with the distance from the sample bottom edge (Figure 2b). As a consequence, the mean energy of the ions decreases with the distance from the edge of the sample (Figure 2); this does not necessarily imply that the local etching rate will also decrease, as it additionally depends on the angle of ion incidence which varies with the distance from the edge (see discussion on IADFs below). The electric potential value does not only affect the mean energy of the ions but also the shape of the IEDFs at 10 mm, that is, due to the low values of the energy, the ions' transition time of the sheath has increased in comparison to the electric field period and the bimodal shape disappears.[40]

The IADFs, shown in Figure 2e,f, are given as a function of the ion incidence angle φ, that is, the angle relative to the normal on the polymeric sample surface. It has to be noticed that for the case of the horizontally placed sample (Figure 2e), the mean ion incidence angle is not 0°, that is, the ions do not impinge

perpendicularly to the surface, due to the fact that the polymeric sample is placed at a distance of 80 mm from the center of the reactor, where the direction of the electric field deviates from the normal to the surface. If the sample was placed at the center of the reactor, the ions would have impinged perpendicularly (i.e., φ would have been 0°).

When placing the polymeric sample perpendicular to the electrode (Figure 2b), the ion incidence angle becomes negative (Figure 2f) at all positions, following the local direction of the electric field (see Figure 2b). At the bottom edge of the perpendicularly placed polymeric sample, the ions are "scratching" the surface of the polymeric sample, with an impinging angle φ greater than 65°. The latter is expected to lead to the formation of ripples parallel to the direction of ions, following previous experimental[36,37] and computational (Monte Carlo and Molecular Dynamics) studies,[31–35] which demonstrate ripple formation at φ greater than a system-dependent critical value, ranging from 60° to 80°. The same studies imply that the nanoripples will be diminished at the other two positions on the polymeric surface (3.3 and 10 mm away from the edge of the sample) as the mean ion incidence angle decreases below ≈65°, leading to a more isotropic roughness pattern. Summarizing, the computational study predicts a change in the roughness pattern as we are getting closer to the bottom edge of the sample: from an isotropic to an anisotropic pattern as φ increases and overcomes ≈65°. Following the same argument, no spatial roughness gradient is expected in the case of the horizontally placed polymeric sample as the mean ion incidence angle is low (below 13°, see Figure 2e).

Having predicted the aforementioned results and their implications on the surface morphology, we proceed to the experimental characterization of plasma micro-nanotextured PMMA substrates that were processed in perpendicular to the reactor electrode position and their comparison with horizontally placed ones.

2.2. Validation of the Predictions via SEM Imaging and Metrology

SEM images for plasma micro-nanotextured PMMA substrates perpendicularly placed on the plasma reactor electrode and at three distances along the z-axis from the substrate bottom edge (at $z \approx 0$, $z \approx 3$, and $z \approx 10$ mm) are shown in **Figure 3**a–c. For comparison, an SEM image of a substrate horizontally placed with respect to the electrode is also displayed in Figure 3d. Roughness is created on the perpendicular surfaces but with a "twist". Near the PMMA bottom edge ($z \approx 0$ mm), that is, near the plasma electrode, roughness is created in the form of nanoripples as predicted from simulation analysis. The anisotropic pattern of nanoripples turns to an isotropic kind of roughness, which is the well-known nanowire-like roughness and bundles, as one moves along the z-axis from the sample bottom edge upward, that is, from $z \approx 0$ to $z \approx 10$ mm. Thus, the variation of the impinging ion angle with the distance from the substrate bottom edge, as predicted by the simulations described earlier, is confirmed to influence the final surface topography. On the contrary, the roughness created on samples horizontally placed in the plasma reactor (as depicted in Figure 3d) does not exhibit any major

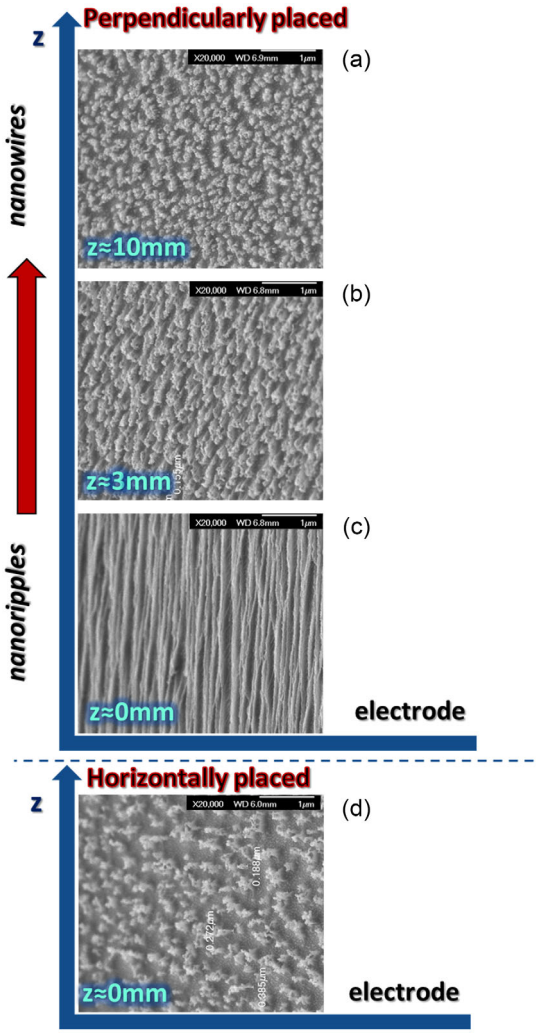

Figure 3. SEM images (45° SEM views) of perpendicularly placed PMMA substrates (plasma etched in ICP mode) of regions at distances a) $z \approx 10$ mm, b) $z \approx 3$ mm, and c) $z \approx 0$ mm from the bottom edge of the substrate and comparison with d) a horizontally placed substrate.

differences from point to point, as expected from the uniformity of IEDFs and IADFs along the substrate (Figure 2c,e).

In order to quantify this transition from anisotropy to isotropy as we are moving upward on the sample, we calculated a properly designed anisotropy index based on the 2D Fourier spectrum of the SEM images of analyzed surfaces (preferably top-down). It is well-known that the anisotropy of a surface morphology is reflected on the Fourier transform (FT) of its SEM image, since FT exhibits contour lines elongated along the anisotropy direction in frequency domain. The degree of elongation of these lines can be used as a metric to quantify the degree of the depicted surface anisotropy. More specifically, we select the contour line corresponding to the 1/3 of the peak of FT, and we calculate the proposed anisotropy index A_{anis} by the following equation:

$$A_{\text{anis}} = 1 - \frac{R_{\min}}{R_{\max}} \tag{1}$$

where R_{min} and R_{max} are the minimum and maximum radius of the selected contour line of FT, respectively. When A_{anis} is close to 0, the analyzed surface is almost isotropic, whereas A_{anis} values close to 1 indicate strong anisotropy of surface morphology with well-formed ripples.

The results of the calculation of A_{anis} from the top-down SEM images correlated with the tilted ones shown in Figure 3 are displayed in **Figure 4**. In the case of the perpendicular sample, a drastic reduction of A_{anis} from 0.8 to 0.1 is noticed as we are moving from the bottom edge ($z \approx 0$ mm) to the top areas of the substrate, characterizing quantitatively the transition from anisotropic to isotropic surface morphologies. At the same bar diagram, for the sake of comparison, we have added the very small value of A_{anis} of the SEM images of samples horizontally placed in plasma reactor justifying the expected isotropy of such surfaces. The previously described transition from isotropic to anisotropic morphologies, for the perpendicularly placed sample, when we approach the bottom edge of the etched polymer sample is accompanied with the emergence of an almost periodic (quasi-periodic) pattern of nanoripples arranged perpendicularly (to the electrode) in a parallel-like manner. This is in agreement with the predictions by Hatsuse et al.[33] where formation of nanoripples parallel to the direction of ions was described for ion incident angles of 75°, as predicted in this work (see computational analysis) at areas very close to the electrode ($z \approx 0$ mm).

The formation of nanoripples is mainly induced by ion reflection effects, as has been studied in previous works on plasma etching of silicon and dielectric materials.[34,36] At high ion incidence angles (>70°), the probability for ion reflection increases and the reflection becomes dominant. The reflected ions are bounced around the neighboring hills on the surface morphology along the ion direction and cause ion channeling effects. Of course, this mechanism requires a preexisting surface roughness (neighboring hills or bumps), which can originate from simultaneous co-deposition of "etch-inhibitors," as has been described in previous works.[41–43] This co-deposition may typically come from sputtering of unetchable "hard inhibitor" materials (metallic or dielectric reactor walls) or from depositing "soft inhibitor" material from the gas phase species.[41]

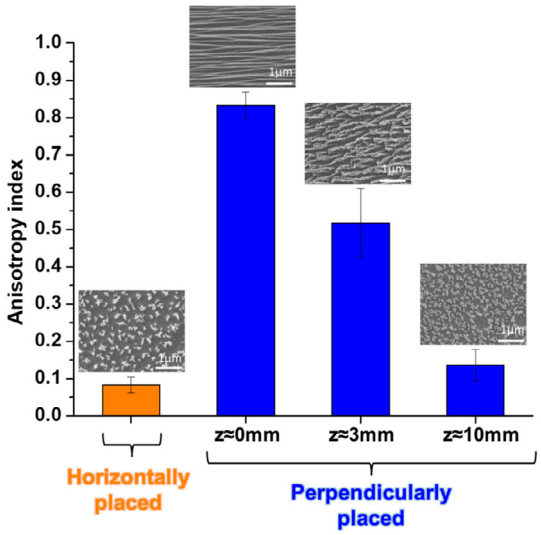

Figure 4. Results of anisotropy index (A_{anis}) of PMMA samples after 3 min plasma treatment (in ICP mode) for horizontally and perpendicularly placed samples in plasma reactor.

Although the ripple formation on samples perpendicularly placed in the plasma reactor seems universal for all plasma modes and materials, some dependence on the substrate material, the plasma process time, as well as the operation mode of the plasma reactor is expected. In **Figure 5**a, the resulting topographies between three samples are compared; two PMMA samples textured in inductively coupled plasma (ICP) and in reactive ion etching (RIE) or capacitively coupled plasma (CCP) mode, respectively, as well as a cyclo-olefin polymer (COP) sample textured in RIE mode. For all samples, the formation of nanoripples is prominently shown in the sample area at $z \approx 0$, rendering this method of texturing polymeric samples, perpendicularly placed in the plasma reactor, rapid, easy and promising for fabricating in one-step (masklessly and without using intricate sheath control plates) quasi-periodic patterns. Furthermore, the dependence of the nanoripple topography on processing parameters, as evidenced from the metrological analysis, follows.

The difference in the nanoripple patterns shown in Figure 5a can be quantified by their period (mean ripple spacing) and their deviation from full periodicity, that is, degree of quasi-periodicity. Both metrics can be estimated by the analysis of the 1D Fourier transform of the image profiles taken perpendicularly to the ripple direction. Indicative results for the mean 1D FT of the profiles of the three images of Figure 5a are shown in Figure 5b. In all cases, the presence of well-defined peaks is noticed and reveals the strong periodicity of the obtained nanoripple patterns. The mean spacing of nanoripples, d, can be calculated from the inverse of the peak of the FT and quantifies the density of the formed nanoripples. The results are shown in **Table 1**, where it can be seen that the patterns obtained in ICP mode are much less dense with a mean ripple spacing almost two times the spacing of RIE patterns (≈180 vs. ≈90 nm). On the contrary, it seems that the change of polymer material has only a slight impact on ripple density causing a reduction from ≈90 nm in PMMA to ≈80 nm in COP substrates (both etched in RIE mode). These observations can be attributed to differences in the etching rate leading to different stages of ripple formation and evolution; the distance between the ripples increases gradually at later stages, induced either by greater etching rates or plasma treatment times. The etching rate is greater in ICP compared to RIE mode (greater ion flux) and under the same mode the etching rate is greater for PMMA compared to COP,[13,16] which can be attributed to the higher etch resistance of COP compared to PMMA due to its cyclic chains.[44] In all cases, the observed periodicities for the polymeric materials studied in this work are consistent with the ones predicted for silicon in the work by Hatsuse et al.[33] where a mean spacing of 35 nm has been obtained at ion incidence angles of 75° (as predicted in this work, for the area adjacent to the electrode), and very close to the periodicities observed for ion beam etching of a photoresist material in the work by Rudiger et al.[24] where periodicities around 100 nm have been recently reported. From the experimental and

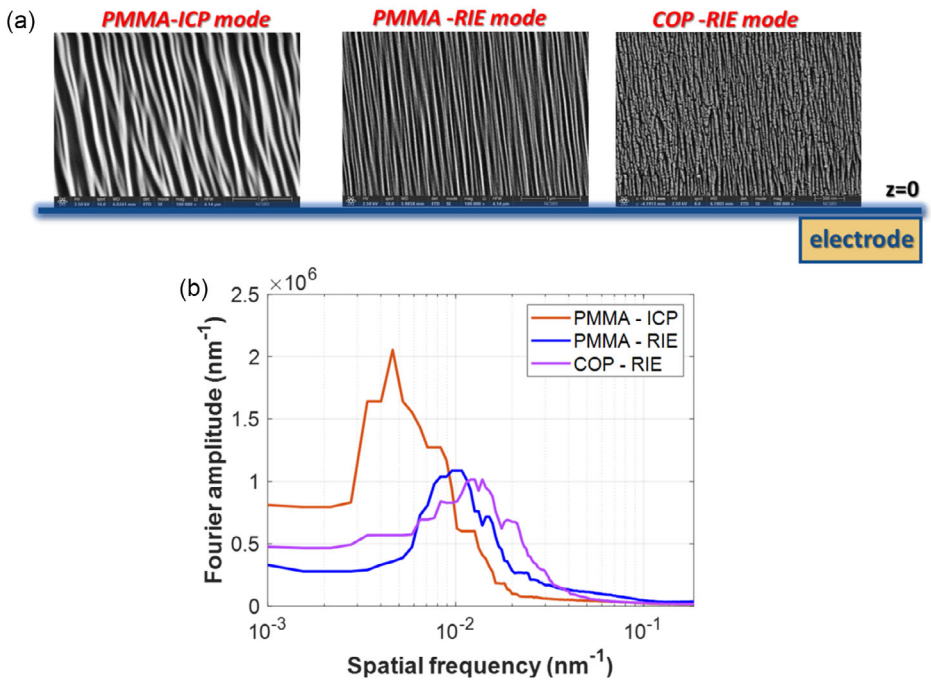

Figure 5. a) SEM images of plasma-textured PMMA and COP samples at different plasma modes; ICP mode (for 3 min), RIE mode (for 5 min). The images indicate universal formation of quasi-periodic nanoripples, and yet some dependence of the periodicity on the plasma processing time, plasma mode (ion concentration), and substrate material. All samples are placed perpendicularly to the plasma electrode. b) The 1D Fourier spectra of SEM image profiles calculated perpendicular to the direction of ripples for PMMA surface etched in ICP (red line) and RIE mode (blue line) and COP etched in RIE mode (purple line). The well-defined peak in all cases justifies the strong periodicity of the obtained nanoripple patterns.

Table 1. Mean spacing (d) and t-disorder parameter (ω) of nanoripples in the anisotropic patterns at the bottom edge of PMMA and COP samples.

Sample	d [nm]	ω
PMMA—ICP mode	186.0 ± 26.3	1.49 ± 0.19
PMMA—RIE mode	89.8 ± 7.8	0.97 ± 0.28
COP—RIE mode	79.2 ± 0.1	1.45 ± 0.24

computational results presented in this work, we can infer that the formation of nanoripples on polymeric substrates is determined by the ion incidence angle which should be higher than 70° for the formation of good periodic structures, while regarding the morphological features of the nanoripples, their mean spacing depends on the material roughness formation rate, which in turn depends mainly on the plasma processing conditions and the material chemical composition.

Furthermore, the deviation of ripple patterns from perfect periodicity was estimated. In the language of the symmetry-based approach to surface metrology, this deviation is termed as the disorder from translational pattern symmetry (t-disorder).[45] A common way to achieve this estimation is the calculation of the normalized width,[46] ω, of the peak shown in the Fourier spectra of Figure 5b. The obtained results for the surfaces of Figure 5a are displayed in Figure 5b and show that the best periodicity is exhibited by the ripple patterns of PMMA material when etched in RIE mode. The other two surfaces have almost identical ω values indicating similar deviations from perfect periodicity. The results of Figure 5 highlight the highly promising capability of the proposed method to generate ripple patterns, offering control over both their density as well as the degree of disorder. Moreover, the term plasma-induced periodic surface structures (PIPSS) is coined for such structures in correspondence with the well-established term laser-induced periodic surface structures[47–49] widely used in the literature for various applications.[50–52] The formation of such nanoripple structures may be achieved, in addition to polymers, on metallic substrates plasma processed in proper gases (e.g., Cl-containing gases).

Finally, in Supporting Information (SI, Section S2), more SEM images are shown where the area over which the nanoripples extend appears to be more than 3 mm in length for PMMA treated in RIE mode and more than 1 mm in ICP mode (see Figure 4). Presumably, the enhanced density of radicals expected in ICP mode reduces the effect of ion-induced nanoripple formation. Therefore, in cases where good pattern uniformity is desired, one can select only this bottom area of the sample and utilize the nanoripple topography accordingly in desirable applications.

3. Conclusion

Herein, reactive plasma etching is proposed as a conventional technological route for rapid, in one-step, maskless, large area,

and mass production of quasi-periodic nanoripples formed on the bottom, adjacent to the electrode, area of polymeric substrates perpendicularly oriented with respect to the electrode surface. A comprehensive modeling framework was utilized for the calculation of the angular and energy distribution of ions reaching the perpendicularly placed substrate with respect to the electrode, providing a justification basis for the proposed strategy. Detailed metrological analysis of SEM images obtained from processed surfaces demonstrates the formation of quasi-periodic nanoripples with density and degree of periodicity depending on the ion density (flux), processing time and to a lesser degree on the polymer material. The orientation and the order of density of such structures as well as their dependence on plasma processing conditions are in agreement with the predictions described in former literature, for ions incident at high angles (75°) and highly reflected from the surface structures. The term PIPSS is coined for such periodic nanostructures created through maskless gaseous plasma processing. As a next step, detailed control of the nanoripple features will be demonstrated and will be exploited in promising material applications. In parallel, the modeling framework will be elaborated and extended by adapting to experimental conditions, relaxing simplifications, and addressing different substrate materials; the aim will be to confirm the validity of the framework and identify the most influential factors for ripple formation.

4. Experimental Section

Modeling Framework and Simulations: The modeling framework includes a reactor scale model and a Monte Carlo particle tracing model. The former is a plasma fluid model[38] and consists of 1) Poisson's equation, 2) the electron and electron energy balance, and 3) the mass balances for all neutral species and ions. The latter calculates the trajectories of the ions by solving Newton's equations of motion.

The aim of the modeling framework is to demonstrate the feasibility and the potential of plasma etching to induce ripples on the perpendicularly placed polymeric samples. As quantitative results are not expected from the modeling framework, we consider a simple Ar plasma (with a simple reaction set to reduce the computational cost) and solve the problem in CCP (RIE) mode as the latter defines the ion energy and angular direction on the substrate. A set of operating conditions was used, but for the results presented herein, the conditions (pressure and self-bias voltage) are close to those of the experiments. A 3D representation of a custom-made plasma reactor[53] used in the calculations (and in the experiments) is shown schematically in Figure 1. On the electrode, which was connected to an RF generator, a circular quartz pane (gray region) was placed. The upper part of the reactor also consisted of quartz. The non-quartz surfaces in contact with the plasma region were metallic grounded walls.

The computational domain for the modeling framework was a 2D slice of the axisymmetric reactor shown in Figure 1. The horizontally (perpendicularly) placed sample had a length of 20 mm and a thickness of 2 mm (4 mm). The reactor pressure was 5.2 mTorr, the gas mixture temperature was considered at 300 K, and the applied RF power (13.56 MHz) at a value to produce a self-bias voltage of −210 V for a capacitively coupled discharge, that is, the reactor operates in RIE mode. The numerical solution is made with COMSOL through a time periodic solver to reduce the very high computational cost of transient problem with time periodic boundary conditions (period ≈74 ns). More details on the model and the solution method are included in the SI.

Materials and Fabrication: The modeling transparent PMMA plates (2 and 4 mm thick) were purchased from IRPEN (Spain), and COP disks were purchased from ChipShop (Zeonex, 2 mm thick) and used as substrates. Isopropyl alcohol (IPA) of molecular biology grade was purchased from Sigma-Aldrich. Deionized water (DI) was used throughout this study.

Polymeric samples were cut into dimensions of 20×10 mm and cleaned with IPA and DI water. Then, they were placed perpendicularly or horizontally inside the custom-made plasma reactor[49] (at a radial distance of 80 mm from the reactor center so that many samples are etched simultaneously) and were oxygen plasma micro-nanotextured. The experimental plasma processing conditions are used as follows: 100 sccm O_2 for a pressure of 5.2 mTorr, and two plasma modes; 600 W source power, 300 W electrode power (−210 V bias voltage), for ICP mode and 0 W source power, 300 W electrode power (−210 V bias voltage), for RIE mode and for various process times.

Metrological Analysis of SEM Images: SEM was conducted with a JEOL/JSM 7401F Field Emission SEM or a ThermoFischer Scientific X/APREO 2S Field Emission SEM for the characterization of the etched polymeric samples that were sputtered coated with 10 nm Pt prior to SEM measurements. Top-down and tilted SEM images were used in a systematic computational analysis in order to characterize the impact of the material and processing conditions on surface morphology. Among the available image magnifications for each surface area, images of magnification ×20 000 were used due to their sufficient statistical information and resolution. At least three images for each perpendicularly placed (on the plasma reactor electrode) substrate and at three distances along the *z*-axis were analyzed (at $z \approx 0$, $z \approx 3$ and $z \approx 10$ mm) to determine the mean value and standard deviation of each metric. The obtained SEM images were also deionized using a median filter with window size 3 pixels. Metrological analysis was conducted to top-down SEM images to calculate the proper metrics for the characterization of surface topographies. It comprises two steps: First, we calculated a properly designed anisotropy index A_{anis} based on Fourier Transform analysis in order to identify the surface topography case, isotropy versus anisotropy (see Equation (1) in main text). Anisotropy index close to 0 indicates a surface that is isotropic, whereas when A_{anis} approaches 1, it reveals strong anisotropic morphologies. In case that A_{anis} is found close to 1, the surface morphology is dominated by ripples forming a periodic-like (i.e., quasi-periodic or disordered) grating. Thus, the second step is to focus on the metrological characterization of the quasi-periodic patterns. The formation of a quasi-periodic pattern is reflected on the 1D Fourier transform calculated from the profiles perpendicular to ripple direction in top-down SEM images. The presence of a well-defined peak reveals the pattern periodicity, while the inverse of the peak frequency provides an estimation of the apparent period (mean spacing) of ripples. Also, the 1D FT can be used for the estimation of the degree of quasi-periodicity (i.e., grating disorder) through the calculation of the normalized full-width half-maximum of the prominent peak. This delivers the value of the *t*-disorder parameter ω quantifying the deviation of the pattern from perfect periodicity. A more complete account of the methodology for the characterization of surface morphology is reported in the Supporting Information.

Supporting Information

Supporting Information is available from the Wiley Online Library or from the author.

Acknowledgements

The authors would like to thank E. Manouras for his assistance with the plasma processing experiments and M-C. Skoulikidou for her assistance with the SEM images. This work was supported by the EU Horizon project VortexLC ("Vortex enhanced liquid chromatography for HbA1c monitoring based diabetes management in a globalized setting," contract no 101047029, www.vortexlc.com). The publication of the article in OA mode was financially supported by HEAL-Link.

Conflict of Interest

The authors declare no conflict of interest.

Author Contributions

Athina S. Kastania: conceptualization (equal); investigation (equal); methodology (equal); project administration (equal); supervision (equal); validation (equal); visualization (equal); writing—original draft (equal); writing—review & editing (equal). **Sotiris Mouchtouris**: investigation (equal); methodology (equal); software (equal); validation (equal); visualization (equal); writing—original draft (equal); writing—review & editing (equal). **Eleni Stai**: investigation (equal); software (equal); validation (equal); visualization (equal); writing—original draft (equal); writing—review & editing (equal). **Angelos Zeniou**: methodology (equal); writing—review & editing (equal). **George Kokkoris**: conceptualization (equal); funding acquisition (supporting); methodology (equal); resources (equal); software (equal); supervision (equal); writing—original draft (equal); writing—review & editing (equal). **Vassilios Constantoudis**: conceptualization (equal); funding acquisition (supporting); methodology (equal); resources (equal); software (equal); supervision (equal); writing—original draft (equal); writing—review & editing (equal). **Pavlos Tsavalas**: visualization (equal); writing—review & editing (equal). **Konstantina Mergia**: resources (equal); visualization (equal); writing—review & editing (equal). **Evangelos Gogolides**: conceptualization (equal); funding acquisition (lead); methodology (equal); project administration (equal); resources (equal); writing—review & editing (equal). **Angeliki Tserepi**: conceptualization (equal); funding acquisition (supporting); methodology (equal); project administration (equal); supervision (equal); writing—original draft (equal); writing—review & editing (equal).

Data Availability Statement

The data that support the findings of this study are available from the corresponding author upon reasonable request.

Keywords

anisotropy ratio, high surface area, inclined polymer surfaces, metrological analysis, modeling framework, nanoripples, reactive plasma etching

Received: November 20, 2024
Revised: January 11, 2025
Published online: February 13, 2025

[1] K. Busch, G. von Freymann, S. Linden, S. F. Mingaleev, L. Tkeshelashvili, M. Wegener, *Phys. Rep.* **2007**, *444*, 101.
[2] H. Yin, K. Xing, Y. Zhang, D. M. A. S. Dissanayake, Z. Lu, H. Zhao, Z. Zeng, J.-H. Yun, D.-C. Qi, Z. Yin, *Chem. Soc. Rev.* **2021**, *50*, 6423.
[3] P. Ragesh, V. Anand Ganesh, S. V. Nair, A. S. Nair, *J. Mater. Chem. A* **2014**, *2*, 14773.
[4] O. Apel, F. Beinhorn, J. Ihlemann, J.-H. Klein-Wiele, G. Marowsky, P. Simon, *Z. Phys. Chem.* **2000**, *214*, 1233.
[5] M. Huang, F. Zhao, Y. Cheng, N. Xu, Z. Xu, *ACS Nano* **2009**, *3*, 4062.
[6] M. Mastellone, A. Bellucci, M. Girolami, V. Serpente, R. Polini, S. Orlando, A. Santagata, E. Sani, F. Hitzel, D. M. Trucchi, *Nano Lett.* **2021**, *21*, 4477.
[7] X. Liang, R. Dong, J. C. Ho, *Adv. Mater. Technol.* **2019**, *4*, 1800541.
[8] X. Xu, Q. Yang, N. Wattanatorn, C. Zhao, N. Chiang, S. J. Jonas, P. S. Weiss, *ACS Nano* **2017**, *11*, 10384.
[9] T. Karabacak, G.-C. Wang, T.-M. Lu, *J. Appl. Phys.* **2003**, *94*, 7723.
[10] I.-T. Chen, E. Schappell, X. Zhang, C.-H. Chang, *Microsyst. Nanoeng.* **2020**, *6*, 22.
[11] A. Tserepi, E. Gogolides, K. Tsougeni, V. Constantoudis, E. S. Valamontes, *J. Appl. Phys.* **2005**, *98*, 113502.
[12] L. T. Phan, S. M. Yoon, M.-W. Moon, *Polymers* **2017**, *9*, 417.
[13] K. Tsougeni, N. Vourdas, A. Tserepi, E. Gogolides, C. Cardinaud, *Langmuir* **2009**, *25*, 11748.
[14] F. Palumbo, R. Di Mundo, D. Cappelluti, R. d'Agostino, *Plasma Processes Polym.* **2011**, *8*, 118.
[15] N. E. Vourdas, M. E. Vlachopoulou, A. Tserepi, E. Gogolides, *Int. J. Nanotechnol.* **2009**, *6*, 196.
[16] K. Ellinas, K. Tsougeni, P. S. Petrou, G. Boulousis, D. Tsoukleris, E. Pavlatou, A. Tserepi, S. E. Kakabakos, E. Gogolides, *Chem. Eng. J.* **2016**, *300*, 394.
[17] C. Alemán, G. Fabregat, E. Armelin, J. J. Buendía, J. Llorca, *J. Mater. Chem. B* **2018**, *6*, 6515.
[18] C. Ma, A. Nikiforov, N. De Geyter, X. Dai, R. Morent, K. Ostrikov, *Prog. Polym. Sci.* **2021**, *118*, 101410.
[19] P. Dimitrakellis, K. Ellinas, G. D. Kaprou, D. C. Mastellos, A. Tserepi, E. Gogolides, *Macromol. Mater. Eng.* **2021**, *306*, 2000694.
[20] K. Tsougeni, A. S. Kastania, G. D. Kaprou, M. Eck, G. Jobst, P. S. Petrou, S. E. Kakabakos, D. Mastellos, E. Gogolides, A. Tserepi, *Sens. Actuators, B* **2019**, *288*, 171.
[21] A. S. Kastania, P. S. Petrou, C. M. Loukas, E. Gogolides, *Biomed. Microdevices* **2020**, *22*, 44.
[22] B. Chang, *Nanotechnology* **2020**, *31*, 085301.
[23] S. A. Cybart, P. Roediger, E. Ulin-Avila, S. M. Wu, T. J. Wong, R. C. Dynes, *J. Vacuum Sci. Technol. B* **2013**, *31*, 010604.
[24] T. Rüdiger, M. Mitzschke, C. Bundesmann, A. Prager, Y. Liu, B. Abel, A. Schulze, F. Frost, *Surf. Coat. Technol.* **2024**, *494*, 131407.
[25] S. Schauer, R. Schmager, R. Hünig, K. Ding, U. W. Paetzold, U. Lemmer, M. Worgull, H. Hölscher, G. Gomard, *Opt. Mater. Express* **2018**, *8*, 184.
[26] S. Augustine, A. Hole, K. P. Sooraj, M. Saini, A. Deshmukh, V. Gota, P. Chaturvedi, M. Ranjan, C. Murali Krishna, *Radiat. Eff. Defects Solids* **2024**, *179*, 1644.
[27] S. Bai, D. Serien, A. Hu, K. Sugioka, *Adv. Funct. Mater.* **2018**, *28*, 1706262.
[28] A. B. Faia-Torres, S. Guimond-Lischer, M. Rottmar, M. Charnley, T. Goren, K. Maniura-Weber, N. D. Spencer, R. L. Reis, M. Textor, N. M. Neves, *Biomaterials* **2014**, *35*, 9023.
[29] Y. Hou, W. Xie, L. Yu, L. C. Camacho, C. Nie, M. Zhang, R. Haag, Q. Wei, *Small* **2020**, *16*, 1905422.
[30] K. Zhou, Y. Li, L. Zhang, L. Jin, F. Yuan, J. Tan, G. Yuan, J. Pei, *Bioact. Mater.* **2021**, *6*, 262.
[31] J. J. Végh, D. B. Graves, *Plasma Sources Sci. Technol.* **2010**, *19*, 45005.
[32] C. F. Abrams, D. B. Graves, *J. Vacuum Sci. Technol. A* **1998**, *16*, 3006.
[33] T. Hatsuse, N. Nakazaki, H. Tsuda, Y. Takao, K. Eriguchi, K. Ono, *J. Appl. Phys.* **2018**, *124*, 143301.
[34] K. Ono, N. Nakazaki, H. Tsuda, Y. Takao, K. Eriguchi, *J. Phys. D: Appl. Phys.* **2017**, *50*, 414001.
[35] H. Tsuda, N. Nakazaki, Y. Takao, K. Eriguchi, K. Ono, *J. Vacuum Sci. Technol.* **2014**, *32*, 031212.
[36] Y. Yin, H. H. Sawin, *J. Vacuum Sci. Technol. A* **2008**, *26*, 151.
[37] N. Nakazaki, H. Matsumoto, S. Sonobe, T. Hatsuse, H. Tsuda, Y. Takao, K. Eriguchi, K. Ono, *AIP Adv.* **2018**, *8*, 055027.
[38] S. Mouchtouris, G. Kokkoris, *Plasma Sources Sci. Technol.* **2016**, *25*, 25007.
[39] S. Mouchtouris, G. Kokkoris, *Plasma Processes Polym.* **2017**, *14*, 1600147.
[40] E. Kawamura, V. Vahedi, M. A. Lieberman, C. K. Birdsall, *Plasma Sources Sci. Technol.* **1999**, *8*, R45.
[41] G. Kokkoris, V. Constantoudis, P. Angelikopoulos, G. Boulousis, E. Gogolides, *Phys. Rev. B* **2007**, *76*, 193405.

[42] E. Gogolides, V. Constantoudis, G. Kokkoris, D. Kontziampasis, K. Tsougeni, G. Boulousis, M. Vlachopoulou, A. Tserepi, *J. Phys. D: Appl. Phys.* **2011**, *44*, 174021.
[43] G. Kokkoris, E. Gogolides, *J. Phys. D: Appl. Phys.* **2012**, *45*, 165204.
[44] K. Fricke, H. Steffen, T. von Woedtke, K. Schröder, K.-D. Weltmann, *Plasma Processes Polym.* **2011**, *8*, 51.
[45] V. Constantoudis, I. Ioannou-Sougleridis, A. Dimou, A. Ninou, M. Chatzichristidi, E. Makarona, *Micro Nano Eng.* **2022**, *16*, 100148.
[46] D. Kontziampasis, V. Constantoudis, E. Gogolides, *Plasma Processes Polym.* **2012**, *9*, 866.
[47] Z. Liu, J. Siegel, M. Garcia-Lechuga, T. Epicier, Y. Lefkir, S. Reynaud, M. Bugnet, F. Vocanson, J. Solis, G. Vitrant, N. Destouches, *ACS Nano* **2017**, *11*, 5031.
[48] J. Bonse, S. Gräf, *Laser Photonics Rev.* **2020**, *14*, 2000215.
[49] S. Durbach, F. T. Krauss, M. Hoffmann, V. Lehmann, H. Reinhardt, J. Sundermeyer, N. Hampp, *ACS Nano* **2022**, *16*, 10412.
[50] X. Sedao, M. V. Shugaev, C. Wu, T. Douillard, C. Esnouf, C. Maurice, S. Reynaud, F. Pigeon, F. Garrelie, L. V. Zhigilei, J.-P. Colombier, *ACS Nano* **2016**, *10*, 6995.
[51] E. Skoulas, A. C. Tasolamprou, G. Kenanakis, E. Stratakis, *Appl. Surf. Sci.* **2021**, *541*, 148470.
[52] S. N. Erkızan, F. İdikut, Ö. Demirtaş, A. Goodarzi, A. K. Demir, M. Borra, I. Pavlov, A. Bek, *Adv. Opt. Mater.* **2022**, *10*, 2200233.
[53] A. Zeniou, A. Smyrnakis, V. Constantoudis, K. Awsiuk, E. Gogolides, *Nanotechnology* **2021**, *32*, 235305.

